Soft Matter

Accepted Manuscript

ROYAL SOCIETY OF CHEMISTRY

www.rsc.org/softmatter

Effects of hydrophobic interaction strength on the self-assembled structures by model peptides

Yan Mu* and Meng Yu

Abstract

Stable and ordered self-assembled peptides nanostructures are formed as a result of cooperative effects of various relatively weak intermolecular interactions. We systematically studied the influence of hydrophobic interaction strength and temperature on self-assembly of peptides with a coarse-grained model by Monte Carlo simulations. The simulation results show a rich phase behavior of peptide self-assembly, indicating that the formation and morphology of peptide assemblies may be tuned by varying temperature and the strength of hydrophobic interaction. There exist optimal combinations of temperature and hydrophobic interaction strength where ordered fibrillar nanostructures are readily formed. Our simulation results not only facilitate the understanding of the self-assembly behavior of peptides at the molecular level, but also provide useful insights into the development of fabrication strategies of high-quality peptide fibrils.

I. Introduction

Proteins and peptides may self-assemble into insoluble amyloid fibrils, which are often associated with many neurodegenerative disorders such as Alzheimer's, Huntington's and Parkinson's disease, Creutzfeld-Jakobs Syndrome, type II diabetes, and others. [1-5] However, many nanoscale biomaterials, including nanospheres [6], nanofibers [7], nanotapes [8], nanotubes [9-11], and hydrogels [12-13], can be built through the self-organization of peptides, which have already been demonstrated for various applications in biomedicine and biotechnology fields due to their inherent biofunctionality and biocompatibility. For examples, peptide scaffolds have been demonstrated to be templates for growth of functional nerve cell networks and even active synapses [14-16]; and peptide hydrogels have shown application potential as drug delivery agents. [17-20] In addition, recent study revealed that the amyloid peptide fibrils are comparable to steel in strength and comparable to silk in mechanical stiffness. [21] These exceptional properties make them candidates for new environment-friendly biomaterials for many potential technological applications. [22-25] Hence, the study of self-organization structures and mechanisms of proteins and peptides is becoming a very promising research field in recent years from biomedicine, biochemistry, chemistry, to nanotechnology, physics and materials science.

Regardless of the diversity in sequence and difference in length, peptides have shown the ability of self-assembling into various fibrillar structures, including Aβ-amyloid fibrils [26-27], collagen [28], actin filaments [29-30] and α-helical coiled-coil self-assembling filaments (SAFs) [31]. In fact, the formation of ordered fibrillar structures via self-assembly of peptides is dependent on environmental conditions. These conditions include, among others, temperature [32-34], pH [35-38], salt type and concentration [39-41], and substrates [42-45]. Under suitable external conditions, the self-assembly process of peptides is dominated by various intermolecular interactions, including van der Waals, hydrophobic, hydrogen bonding and electrostatic interactions. The ordered self-assembled peptide structures are formed as a result of

the cooperative effects of these different intermolecular interactions. Particularly, the interplay between backbone hydrogen bonding and hydrophobic interaction among amino acid side-chains is crucial to the formation of β-sheet-rich fibrillar structures. [46-50] The backbone hydrogen bonding leads to the skeleton formation of β-sheets, while the hydrophobic interaction between side chains drives individual peptides to oligomers and the subsequent growth into fibrils; and furthermore, the hydrophobic interaction account for the stabilization of the ordered peptide assemblies. Han *et al*. investigated the influences of hydrophobic and hydrogen bonding interactions on the self-assembly of short amphiphilic peptides (I_mK and L_mK, where I denotes isoleucine, L denotes leucine and K denotes lysine). It was found that the shape and size of self-assembled nanostructures by those short peptides can be altered by the rearrangement of amino acid residues and the hydrophobic chain length. [47] Meijer *et al*. studied the effects of the hydrophobic interactions on both stabilization and morphology of fibrillar assemblies formed by amphiphilic peptides (KTVIIE, where T denotes threonine, V denotes valine and E denotes glutamic acid) with alkyl tails. Their experimental results indicated that the thermal stability of the fibrillar assemblies can be increased by introducing n-alkyl groups, without altering the peptide aggregates morphology. [46] Very recently, Ni *et al*. studied the dependence of self-assembly of fibril-forming polypeptides on temperature and residue hydrophobicity with a coarse grained model via lattice Monte Carlo method. They discovered a strong coupling between the hydrophobic-interaction-driven polypeptide folding and assembling. They also found that there was a strong dependence of the formation and growth of fibril structures on the hydrophobicity of specific residues and temperature. [50] From the above studies, it can be seen that the strength of hydrophobic interaction between amino acid side chains is a very important parameter governing the aggregation process and self-assembled structure of peptides. Therefore, understanding how hydrophobic interaction strength affects the self-assembling behavior of peptides is a critical step towards the manipulation of the size and shape of the final self-assembled peptide structures.

In this paper, we investigated the influences of both the strength of hydrophobic interaction and temperature on the aggregation process and self-assembled structure of model peptides with nonpolar side chains by computer simulations. The subsequent sections of this paper are organized as follows. In section II, we introduce briefly our improved coarse-grained model for polypeptide. In section III, simulation results are presented with discussion. Conclusions are drawn in section IV based upon our results.

II. Model and method:

While in principle all-atom models can provide more detailed information on the folding and aggregation structures, it is extremely time consuming for studying the self-assembly process of peptides by long time and large size simulations due to the high degree of complexity of aggregation process. In the present study, an improved coarse-grained four-bead model based on our earlier work is used to describe the amino acids in peptides. Each amino acid residue is composed of four united atoms: N, C_α, C, and side chain R, as shown in Figure 1. In previous four-bead models [51-52], the hydrogen and oxygen atoms, which are respectively embedded in the united atoms N and C, are implicit in all (including hydrogen bonding) interactions. The hydrogen bonding potential functions used in the previous four-bead models are too oversimplified to reflect the geometry of hydrogen bond accurately due to artifacts. In the current four-bead model, a more realistic hydrogen bonding potential fitted from protein data bank is employed. [53] This hydrogen bonding potential consists of distance and angle components which can capture the structural features of hydrogen bond accurately. The hydrogen and oxygen atoms are explicit in this hydrogen bonding interaction, but are implicit in the excluded volume effects. This treatment significantly reduces simulation time without losing the resolution on the structural characteristics of peptides assemblies. Using this highly efficient coarse-grained four-bead model, we had successfully simulated the spontaneous formation of

left-handedly twisted fibril-like structures of amyloid-forming peptide (GGVVIA) in solution [54] and studied the effects of surface hydrophobicity on the conformational changes of different length model polypeptides with hydrophobic side chains [55].

The total potential energy of the system in the current study is given by:

$$E = E_{ex} + E_{hb} + E_{hp} \quad (1)$$

where E_{ex}, E_{hb} and E_{hp} are the excluded volume effects, the hydrogen bonding and the hydrophobic interactions, respectively. The excluded volume effect is modeled by a hard-sphere potential, which applies to all possible united atom pairs, except those consisting of two united side chain atoms, i.e., two "*R*"s. The interaction between the united side chain atoms is characterized by the hydrophobic interaction potential instead. For local hard-sphere interactions between the united atoms separated by three or fewer bonds along the chain, the diameters of these atoms themselves are more appropriate than the effective diameters of united atoms [51]. Therefore, those united atoms separated by three or fewer bonds along the chain are allowed to overlap by up to 25% [52] in the present model. The corresponding diameter of each united atom is also listed in Table I.

The hydrogen bonding interaction takes the following form [53]:

$$E_{hb} = \varepsilon_{hb} \sum_{ij} u(r_{ij}) v_1(\theta_{1,ij}, \theta_{1,avg}) v_2(\theta_{2,ij}, \theta_{2,avg}) v_3(\theta_{3,ij}, \theta_{3,avg}) \quad (2)$$

where $u(r)$ and $v(\theta)$ are the distance and angle components of the potential, respectively, and

$$u(r_{ij}) = 5\left(\frac{\sigma_{hb}}{r_{ij}}\right)^{12} - 6\left(\frac{\sigma_{hb}}{r_{ij}}\right)^{10} \quad (3)$$

$$v_n(\theta_{n,ij}, \theta_{n,avg}) = \begin{cases} \frac{1}{3}\left[4\cos^2(\theta_{n,ij} - \theta_{n,avg}) - 1\right], \theta_{n,ij} < (\theta_{n,avg} + \Delta\theta), n = 1,2,3 \\ 0 \quad , \quad otherwise \end{cases} \quad (4)$$

where r_{ij} is the distance between H_i and O_j, and σ_{hb} is 1.80Å as the average hydrogen bond length. In the present model, the H and O atoms are embedded in the united

atoms N and C, respectively, and are implicit in the excluded volume effects. However, their coordinates are calculated and used for the determination of hydrogen bonding interaction in the simulations. To speed up the simulations, a cutoff radius r_c = 5.0Å is used in the current model. $\theta_{1,ij}$, $\theta_{2,ij}$ and $\theta_{3,ij}$ are $\pi - \angle NHO$, $\pi - \angle COH$, and the acute angle between $\overrightarrow{NH}$ and $\overrightarrow{OC}$ vectors, respectively. $\theta_{n,avg}$ (n = 1, 2, 3) are their averages which take the values of 17.98˚, 26.77˚ and 11.60˚, respectively. To increase the efficiency of hydrogen bond formation, an uncertain deflection angle $\Delta\theta$ = 60˚ is required. In addition, to increase the efficiency of hydrogen bond formation, we allow for the overlap between united atoms N and C by up to 15%. ε_{hb} is the strength of the hydrogen bonding interaction and is set to be unity. In the current work, all energy parameters are in units of ε_{hb}, while reduced temperature T^* is in units of ε_{hb}/k_B, where k_B is the Boltzmann constant.

Besides the hydrogen bonding interaction, the hydrophobic interaction between nonpolar side chains plays a critical role in the formation and stabilization of ordered self-assembled structures of peptides. In the original four-bead coarse-grained models, the hydrophobic interaction is generally described by the simple square-well potentials. In the current study, the hydrophobic interaction between side chains is described by the Lennard-Jones potential function:

$$E_{hp} = \varepsilon_{hp} \sum_{ij} \left[\left(\frac{\sigma_{hp}}{r_{ij}} \right)^{12} - 2 \left(\frac{\sigma_{hp}}{r_{ij}} \right)^{6} \right] \quad (5)$$

where r_{ij} is the distance between hydrophobic side chains i and j, and σ_{hp} is the distance corresponding to the minimum hydrophobic potential. ε_{hp} is the corresponding hydrophobic interaction strength. All united side chain atom R are rigidly attached to C_α atoms and held in positions relative to the backbone so that all residues are *L*-isomers. Considering realistic movement of side chains, the distances from R to N and C are allowed to fluctuate within 2.5% of their corresponding bond lengths listed in Table I.

In our Monte Carlo simulations, the conformational change and move of peptides are described by three motion styles, including center of mass translation, pivot and fixed end moves. The pivot move can change the conformation of peptide in a relatively large size by altering backbone torsional angles φ and ψ. The fixed end move changes the conformation of individual peptide by rotating a segment between two randomly chosen C_α atoms and keeping the atoms outside this segment fixed, which is very effective in changing conformations of individual polypeptide in a gentle way. It merely alters the bond angle α besides the torsional angles φ and ψ. The allowed range of the bond angle α is set to [α_0-10˚, α_0+10˚], where α_0 is the average value of α and is set to 111.0˚ [56]. Thus, the degrees of freedom per amino acid in the current model include the two Ramachandran torsional angles φ and ψ, and the bond angle α. All bond lengths, bond angles β and γ, and torsional angle ω (which is restricted to 180˚, corresponding to the *trans* conformation of the amide plane) are fixed. The bond lengths and angles used in our simulations are listed in Table I.

III. Results and discussion

In the current study, a model peptide with the sequence HHHHHH was considered. Here H denotes a generic hydrophobic amino acid, which can be characterized by given hydrophobic interaction strengths (ε_{hp}). By adjusting the diameter of the side chain united atom R, this generic hydrophobic amino acid H may therefore describe various hydrophobic amino acids, such as alanine or valine. Based on the diameter value of the side chain listed in Table I, the current model peptide corresponds to polyalanine. The ground state of the model peptide is α-helix at low temperatures. Each system contains 50 peptides, and the peptide concentration was fixed at 10 mM. All simulations were performed in a cubic box with three-dimensional periodic boundary conditions. Initial conformations of all peptides were random coils for each simulation. The peptides were randomly dispersed in the simulation box. A short Monte Carlo simulation at very high temperature ($T^* = 0.5$) was carried out to eliminate any steric conflicts occurred during system setup. In each simulation, 4×10^7

MC steps were run to reach system equilibration and another 2×10^7 MC steps for data collection. All statistical results were averaged from at least five independent simulations for each set of system parameters. The error bars were derived from the standard deviations.

With varying hydrophobic strength ε_{hp}, diverse self-assembled structures of peptides were observed in the simulations. Four representative aggregation structures were obtained at different ε_{hp}: amorphous aggregates, single-layered β-sheets, amorphous β-sheet aggregates, and fibrillar structures (twisted multi-layered β-sheets). Here, amorphous aggregates refer to the disordered aggregation structures (i.e., the mixtures of different secondary structures). Amorphous β-sheet aggregates refer to the aggregation structures mainly composed of single-layered β-sheets, where the β-sheets are in a disordered arrangement and their content is more than 50%. The fibrillar structures refer to the twisted ordered multi-layered β-sheets. Figure 2 shows these representative aggregation structures obtained in our simulations.

To reveal the influences of the hydrophobic interaction strength ε_{hp} and temperature on the self-assembled structures of the model peptides, we calculated the percentages of peptides forming various secondary structures as a function of reduced temperature T^* at different ε_{hp}. Figure 3a shows the percentages of peptides involving in different secondary structures in the weak-ε_{hp} system where $\varepsilon_{hp} = 0.05$. The representative system snapshots at different temperatures are shown in Figures 3b-3d. At the relatively weak hydrophobic interaction strength and low temperatures ($T^* < 0.09$), most peptides assumed the ground state, i.e., the α-helical structures (Fig. 3b). The weak hydrophobic interactions are insufficient to hold the peptides in close vicinity with one another, and thus cannot drive the peptide aggregating. Some of the α-helices gradually denatured and transformed into random coils with increasing temperature ($0.09 \le T^* < 0.11$), which facilitates the inter-molecular hydrogen bond formation and leads to the formation of β-sheets. However, driven by the weak

hydrophobic interactions, the peptides can merely self-assemble into single-layered β-sheets, and the growth of β-sheets is only through attracting individual peptides into their ends. The highest fraction of peptides forming single-layered β-sheets is about 38% at $T^* = 0.095$ (Fig. 3c). At high temperatures ($T^* \geq 0.11$), random coils are the dominant structures due to strong thermal fluctuations (Fig. 3d). Individual β-hairpins are rarely formed in the whole temperature region.

The aggregation behaviors and the resultant structures become complicated as the hydrophobic interaction strength is increased. In the system with intermediate ε_{hp} where $\varepsilon_{hp} = 0.10$, the formation of aggregates, especially ordered β-sheets, was enhanced significantly. Figure 4a shows the percentages of peptides forming various secondary structures in the overall system. Figure 4b shows the percentages of peptides involved in different secondary structures within the aggregates. The representative snapshots of the system at different temperatures are shown in Figures 4c-4f. As is shown in Figure 4a, the combination of relatively strong hydrophobic interactions ($\varepsilon_{hp} = 0.10$) and moderate temperatures ($T^* < 0.115$) is in favor of the peptide aggregate formation. However, at around $T^* = 0.085$ an abrupt decrease in aggregate content occurred, corresponding to a structural transition from the amorphous aggregates to the β-rich fibrillar structures. As is shown in Figure 4b, the aggregation structures at low temperatures ($T^* \leq 0.085$) are disordered amorphous aggregates, which are mainly composed of α-helices or mixtures of various secondary structures (Figs. 4c and 4d). With increasing temperature, the probability of inter-molecular hydrogen bond formation between peptides within the aggregates is enhanced with the help of thermal fluctuations, while the intermediate hydrophobic interactions is still sufficient in holding the peptides close to each other. The re-positioning and adjustments of peptides into fibrillar structures excluded the non-participating peptides, which reduced the aggregate size and gave rise to an enhancement of individual α-helices at $T^* = 0.085$ (Figure 4a). As the temperature further increases, the β-rich fibrillar structures continued to expand by self-adjusting

and combining free individual peptides. As a result, in the intermediate temperature region of $0.085 < T^* \leq 0.115$, the β-sheets become the dominant structures in the aggregates and ordered fibrillar structures (i.e. twisted multi-layered β-sheets) appeared (Fig. 4e). At high temperatures ($T^* > 0.115$), the peptides basically assumed random coils due to strong thermal fluctuations (Fig. 4f). The α-helices content peaks at two temperatures, as shown in Fig. 4a. The first peak is at $T^* = 0.085$, corresponding to the structural transition from the amorphous aggregates to the β-rich fibrillar structures, while the second low peak appears at $T^* = 0.115$, corresponding to the phase transition between aggregation structures and random coils. Individual β-hairpins are still rarely formed in the whole temperature region.

Aggregate formation becomes even more prominent at enhanced ε_{hp}. Figure 5a shows the percentages of peptides forming various secondary structures in the enhanced-ε_{hp} system where $\varepsilon_{hp} = 0.15$. Figure 5b shows the percentages of peptides forming different secondary structures within aggregates. The representative snapshots of the system at different temperatures are shown in Figures 5c-5g. Apparently, due to the enhanced hydrophobic interactions, nearly all peptides were involved in aggregates at low-to-mid temperatures up to $T^* = 0.12$. Similar to the counterpart system with $\varepsilon_{hp} = 0.10$, the aggregates at low temperatures ($T^* \leq 0.10$) are mainly composed of α-helices or mixtures of various secondary structures (Figs. 5c and 5d), while the fibrillar structures were formed in the intermediate temperatures of $0.10 < T^* \leq 0.125$ (Figs. 5e and 5f). Comparing Figs. 4e with 5f, the fibrillar structures include more β-sheet layers at higher ε_{hp}. At high temperatures ($T^* > 0.125$), random coils are the dominant structures due to strong thermal fluctuations (Fig. 5g). The transition from aggregation structures to random coils is very sharp, as shown in Fig. 5a. In addition, individual α-helices and β-hairpins are nearly not present in the whole temperature region.

Figure 6a shows the percentages of peptides forming various secondary structures

in system where ε_{hp} = 0.20. Figure 6b shows the percentages of peptides in different secondary structures within aggregates. The representative snapshots of the system at different temperatures are shown in Figures 6c-6f. As shown in Fig. 6a, again, all peptides were involved in the aggregation structures due to the very strong hydrophobic interactions at low-to-mid temperatures until T^* = 0.13. The fraction of aggregates subsequently drops to zero at T^* = 0.15. At low temperatures ($T^* \leq 0.10$), the aggregation structures are mainly a mixture of various secondary structures, i.e., amorphous aggregates (Fig. 6c). In the intermediate temperature region of $0.10 < T^* \leq 0.135$, the content of β-sheets in the aggregates is greater than 50%, with a peak of 80% appearing at T^* = 0.12. However, in contrast to the ordered arrangement of β-sheets in the fibrillar structures, the β-sheets in the current aggregates are arranged in a disordered fashion; in other words, the current aggregation structures are amorphous β-sheet aggregates to a large extend (Fig. 6d). It should be noted that no fibrillar structures was formed in the current system with ε_{hp} = 0.20. As temperature is further increased ($0.135 < T^* \leq 0.1475$), the aggregates are mainly composed of random coils, suggesting that the aggregation structures disassociated (Fig. 6e). As shown in Fig. 6f, random coils become the dominant structures when $T^* \geq 0.15$ due to strong thermal fluctuations. Individual α-helices and β-hairpins were rarely observed in the whole temperature region.

To further quantitatively elucidate the effects of hydrophobicity of residues on the structural transition, we calculated the specific heat via energy fluctuations as a function of reduced temperature. [57] At the weak hydrophobic interaction strength ε_{hp} = 0.05, as shown in Fig. 7a, the specific heat has only one peak at T^* = 0.10, corresponding to the phase transition from the single-layered β-sheets to disordered random coils. As ε_{hp} is increased to 0.10, the specific heat has two peaks (Fig. 7b): the first broad peak at the lower temperature T^* = 0.09 corresponds to the structural transition from the amorphous aggregates to the fibrillar structures, while the second sharp peak at the higher temperature T^* = 0.115 displays the phase transition from the

fibrillar structures to disordered random coils. When ε_{hp} is further increased to 0.15, the amplitude of the first peak reduces, indicating reduced energy differences between the amorphous aggregates and the fibrillar structures; while the amplitude of the second peak enhances substantially (Fig. 7c), suggesting that the stabilities of the aggregation structures are enhanced with increasing ε_{hp}. At the strong hydrophobic interaction strength ε_{hp} = 0.20, as shown in Fig. 7d, the specific heat has only one sharp peak at T^* = 0.1475, corresponding to the phase transition from the amorphous aggregates to disordered random coils. In addition, as shown in Figs. 7a-7d, the phase transition temperature between aggregation structures and disordered random coils increases linearly with ε_{hp}, indicating that the hydrophobic interactions play important role in the stabilization of aggregation states.

Based on the above simulation results, a T^*-ε_{hp} phase diagram is developed and shown in Figure 8. The data points represented by the filled circles are the phase transition temperatures between the ordered aggregation structures and random coils. The data points represented by the filled squares are the structural transition temperatures below which α-helical structures and amorphous aggregates are the stable structures. Overall, the phase diagram is divided into three regions by the two transition temperature curves when the hydrophobic interaction strength $\varepsilon_{hp} \leq 0.175$. Deriving from the above simulation results, the top region above the higher curve is where disordered random coils are the dominant structures; the middle region between the two curves is further divided into three sub-regions from left to right, namely, single-layered β-sheets, fibrils and amorphous β-sheet aggregates, respectively; and the bottom region below the lower curve is divided into two sub-regions, which are α-helices and amorphous aggregates. In the right part of the phase diagram where $\varepsilon_{hp} > 0.175$, there is an additional amorphous aggregate region at high temperatures between amorphous β-sheet aggregate and random coils due to the strong hydrophobic interactions. The filled triangle represents the phase transition temperature between the amorphous aggregate and amorphous β-sheet aggregate. The

curves are extrapolated beyond the T^*-ε_{hp} of study, which are represented by dashed lines. The values of ε_{hp} at which those sub-regions are determined are somehow arbitrary. Rather than representing phase equilibrium between two phases, they only serve as a general guideline as they were determined by direct comparison of the final aggregation structures at different ε_{hp} via visual observations. It should be noted that at very low temperatures, the systems may be trapped in local minima for a very long time due to insufficient thermal fluctuations. Nevertheless, this phase diagram helps on understanding the effects of hydrophobic interaction strength and temperature on the self-assembly behavior of peptides with nonpolar side chains.

As indicated by Fig. 8, the hydrophobic interactions play critical roles not only in peptide aggregation process, but also in the resultant aggregation structures. The relatively weak hydrophobic interactions may drive the peptides self-assembling into merely single-layered β-sheets, while too strong hydrophobic interactions lead to the formation of amorphous β-sheet aggregates. The ordered fibrillar structures can be readily formed at the appropriate intermediate hydrophobic interaction strengths and temperatures. The growth of these ordered fibrillar structures is through both β-sheet elongation and lateral addition of β-sheets. Possible optimal ε_{hp}-T^* windows that are in favor of ordered fibrillar structure formation can be determined from the above phase diagram. Our simulation results are qualitatively in accord with other simulation and experimental observations. In the simulations of Nguyen and Hall [58], it was found that aggregate structures of polyalanines were sensitive to temperature and the ratio R between hydrophobic strength and hydrogen bonding strength. Fibrillar aggregates were formed only at moderately high temperature and the relatively low ratio R = 1/10 or 1/8, while amorphous aggregates were formed at the relatively high ratio R = 1/6. Our phase diagram shows that the ratio region where the fibrillar structures can be formed is from 0.075 to 0.175, which is in good agreement with Nguyen and Hall's simulations. Experimentally, Bernacki and Murphy observed that polyalanine peptides containing between 7 and 25 alanines were trapped in amorphous oligomers at room

temperature (25℃); while at high temperature (60℃), the polyalanines containing 19 alanines associated into fibrillar rather than amorphous aggregates. [59] Similarly, Blondelle and coworkers found that the hydrophobic interaction between the alanine side chains not only drove aggregation of polyalanine-based peptides, but also stabilized the self-assembled structures. Meanwhile, the formation and growth of fibrils was significantly enhanced upon temperature elevation. [60] Very recently, Bowers and coworkers studied the aggregation process of six short peptides that are NNQQNY mutants: NVVVVY, NVVQIY, NVQVVY, NNVVNY, VIQVVY, and NNVVNV. [61] They found that only NVVVVY aggregates quickly and forms long fibrils with well-defined morphology at room temperature due to its strong hydrophobic core; while the other peptides only form short fibrils with poorly defined morphologies or amorphous aggregates. These experimental findings clearly show that the peptide fibril-formation capability is weakened as the hydrophobicity of peptide hydrophobic core is reduced. From a qualitative stand point, our simulation results are in accord with the experimental findings and should provide useful insights into understanding the dependence of peptides self-assembly on the hydrophobic interaction strength between nonpolar side chains.

IV. Conclusions

In summary, we systematically studied the influence of hydrophobicity of residues and temperature on the self-assembly of peptides with a coarse-grained model by Monte Carlo simulations. We found that both temperature and the hydrophobic interaction strength play critical roles in the formation of ordered fibrillar structures. The peptides generally agglomerate into amorphous aggregates composed of a mixture of various secondary structures at low temperatures, while at high temperatures disordered random coils are the dominating structures due to strong thermal fluctuations. There exist optimal intermediate temperatures where the fibrillar structures are prone to be formed. Within the optimal intermediate temperature region, only a few short single-layered β-sheets are formed at the weak hydrophobic

interaction strength ($\varepsilon_{hp} \leq 0.075$). At the intermediate hydrophobic interaction strengths ($0.075 < \varepsilon_{hp} \leq 0.175$), ordered fibrillar structures are readily formed through β-sheet elongation and lateral addition. However, as the hydrophobic interaction strength ε_{hp} is further increased to be > 0.175, only amorphous aggregates and amorphous β-sheet aggregates are present at low and intermediate temperatures due to strong intermolecular attraction. Our simulation results indicate that the structure and morphology of peptide self-assembly can be tuned by changing temperature and the hydrophobicity of residues. There exist optimal combinations of the strength of hydrophobic interaction and temperature at which the ordered β-rich fibrillar structures can be readily formed.

Although the simulation results in the present study are based on a coarse-grained peptide model, they show a rich phase behavior of peptide aggregation depending on temperature and the strength of the hydrophobic interaction, and provide a generic picture for understanding formation mechanism of peptide fibrils at molecular level, which might be used to explain related experimental observations. From an application viewpoint, the present study may provide guidance on fabricating high-quality biological fibril materials by controlling self-assembled structures and morphologies of peptide assemblies. Based on the understanding in the influence of hydrophobic interaction strength on the self-assembly behaviors of peptides, our future studies will focus more on exploiting the impact of the sequence of hydrophobic residues on the fibrillization process of peptides, which may provide useful insights on the design of peptide fibril fabrication strategies.

Acknowledgment:

This work was supported by the National Natural Science Foundation of China (Grant No. 11274122).

Table:

Table I: Geometry parameters.

Bond lengths	(Å)
N-C_α	1.460
C_α-C	1.510
C-N	1.330
C_α-R	1.531
N-R	2.44
C-R	2.49
Bond angles	**(degree)**
$NC_\alpha C$ (α)	111.0
$C_\alpha CN$ (β)	116.0
CNC_α (γ)	122.0
United-atom diameters	**(Å)**
N	3.300
C_α	3.700
C	4.000
R	4.408

Figure Captions:

Figure 1. A schematic picture of a unit amino acid residue based on our coarse-grained peptide model. α, β and γ are the three bond angles. φ and ψ are the two Ramachandran torsional angles.

Figure 2: Representative snapshots of peptide aggregation structures obtained in simulations: (a) amorphous aggregate, (b) single-layered β-sheet, (c) fibrillar structure, and (d) amorphous β-sheet aggregate.

Figure 3: (a) The percentages of peptides forming various secondary structures in system at the hydrophobic interaction strength $\varepsilon_{hp} = 0.05$ as a function of temperature; representative final snapshots of the system at different temperatures: (b) $T^* = 0.08$, (c) $T^* = 0.095$, and (d) $T^* = 0.12$.

Figure 4: The percentages of peptides forming various secondary structures (a) in system and (b) involved in the aggregates at the hydrophobic interaction strength $\varepsilon_{hp} = 0.10$ as a function of temperature; representative final snapshots of the system at different temperatures: (c) $T^* = 0.07$, (d) $T^* = 0.085$, (e) $T^* = 0.10$ and (f) $T^* = 0.12$.

Figure 5: The percentages of peptides forming various secondary structures (a) in system and (b) involved in the aggregates at the hydrophobic interaction strength $\varepsilon_{hp} = 0.15$ as a function of temperature; representative final snapshots of the system at different temperatures: (c) $T^* = 0.09$, (d) $T^* = 0.10$, (e) $T^* = 0.11$, (f) $T^* = 0.12$, and (g) $T^* = 0.13$.

Figure 6: The percentages of peptides forming various secondary structures (a) in system and (b) involved in the aggregates at the hydrophobic interaction strength $\varepsilon_{hp} = 0.20$ as a function of temperature; representative final snapshots of the system at

different temperatures: (c) $T^* = 0.10$, (d) $T^* = 0.12$, (e) $T^* = 0.14$, and (f) $T^* = 0.15$.

Figure 7: The specific heat versus reduced temperature at different hydrophobic interaction strengths: (a) $\varepsilon_{hp} = 0.05$, (b) $\varepsilon_{hp} = 0.10$, (c) $\varepsilon_{hp} = 0.15$, and (d) $\varepsilon_{hp} = 0.20$.

Figure 8: Phase diagram of the system in the T^*-ε_{hp} plane.

Figures:

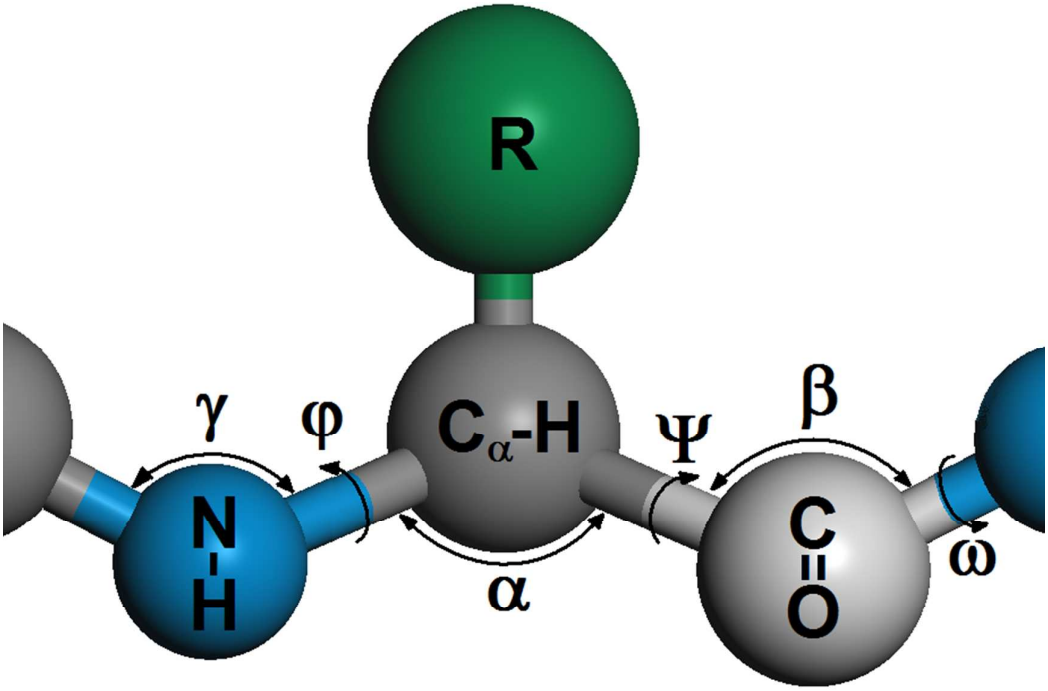

Figure 1

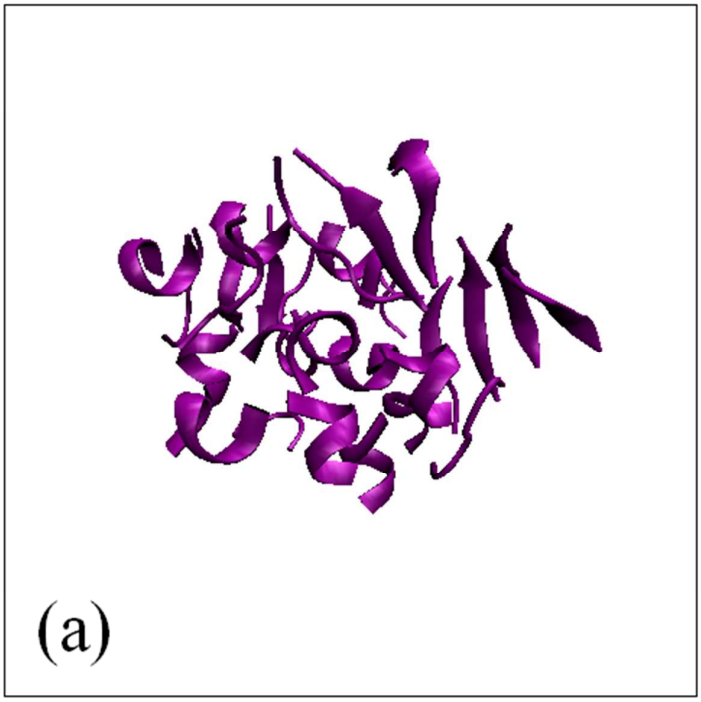

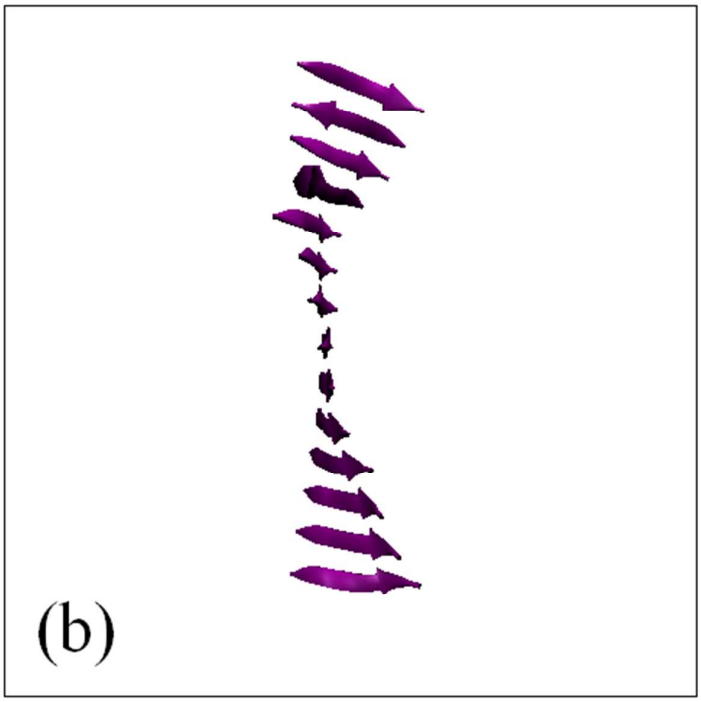

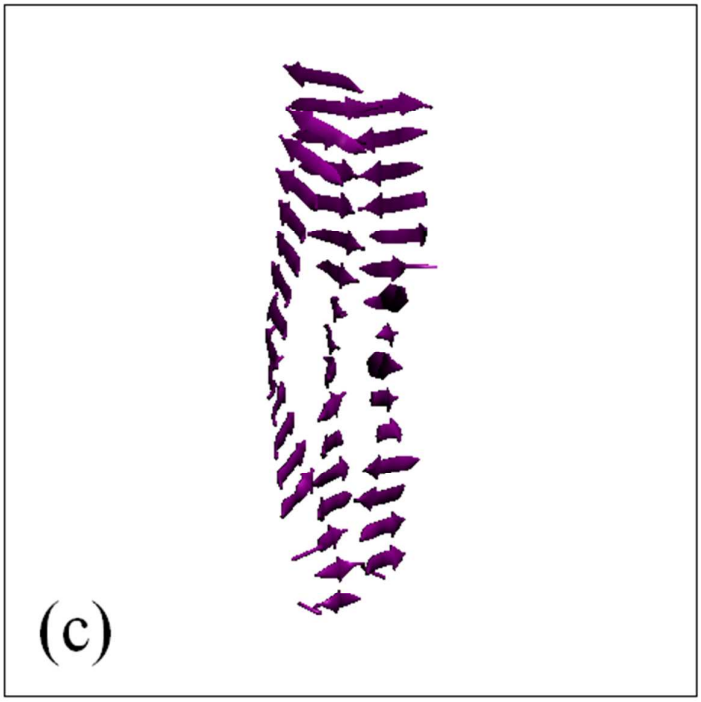

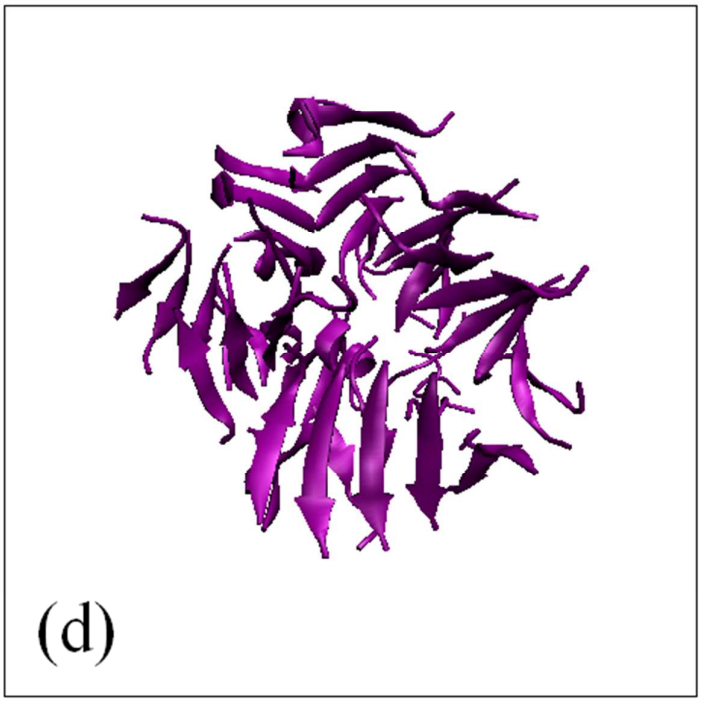

Figure 2

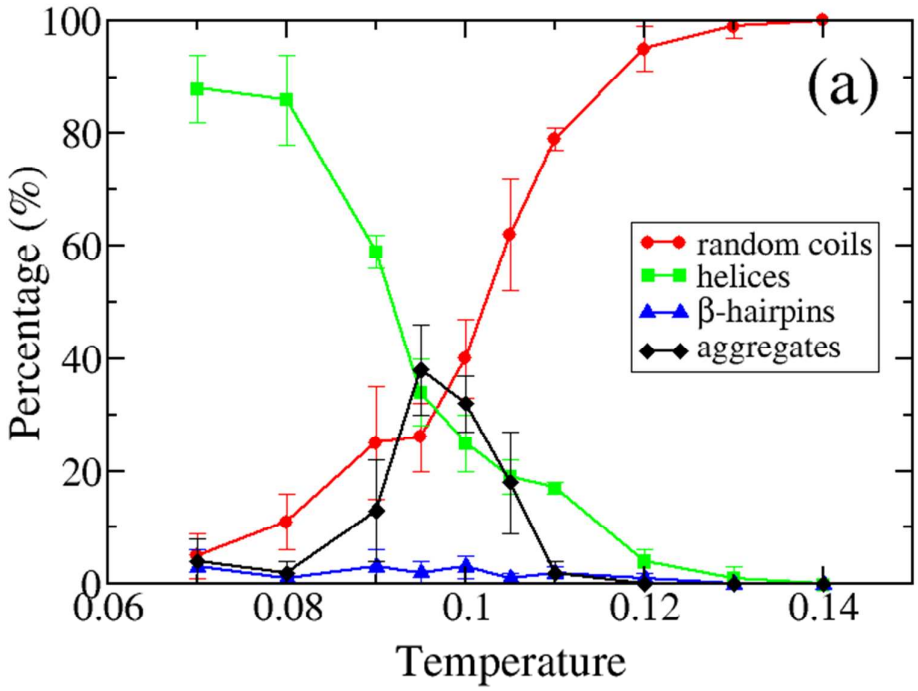

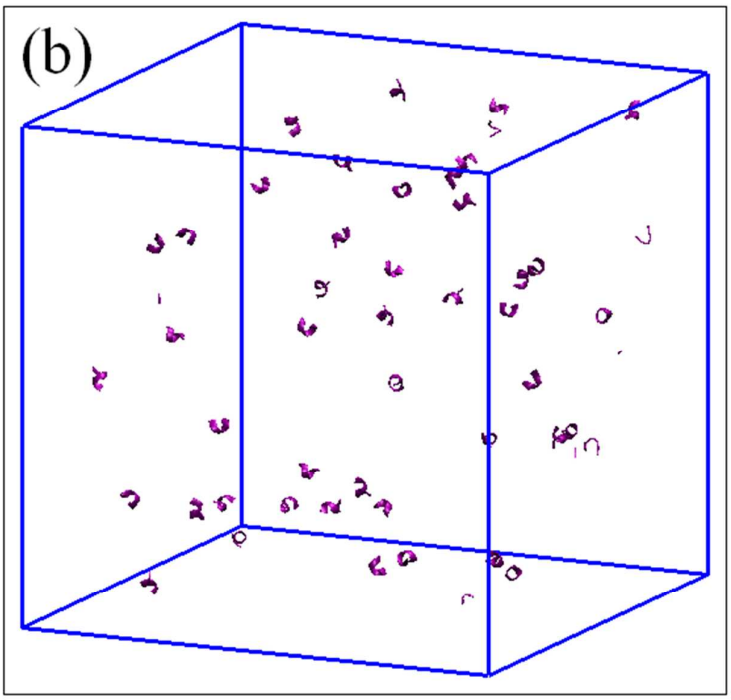

$T^* = 0.08$

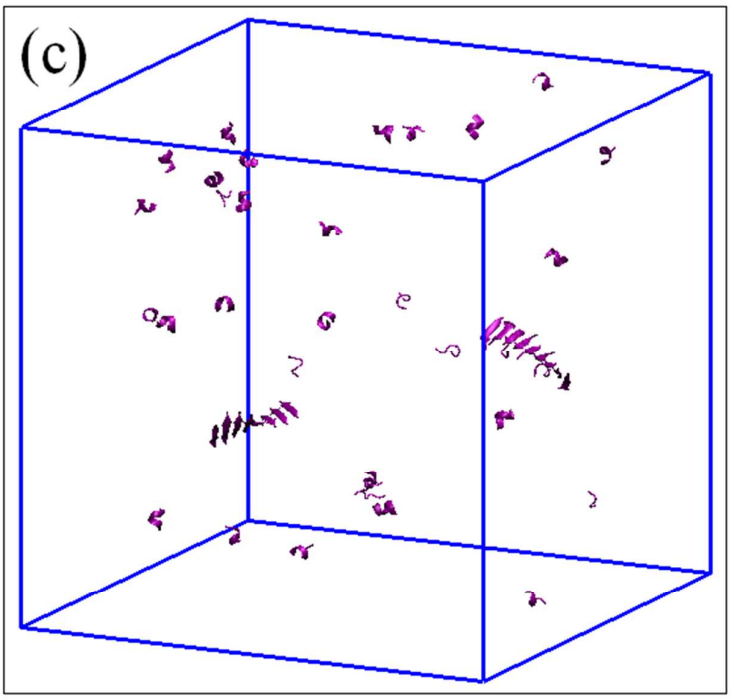

$T^* = 0.095$

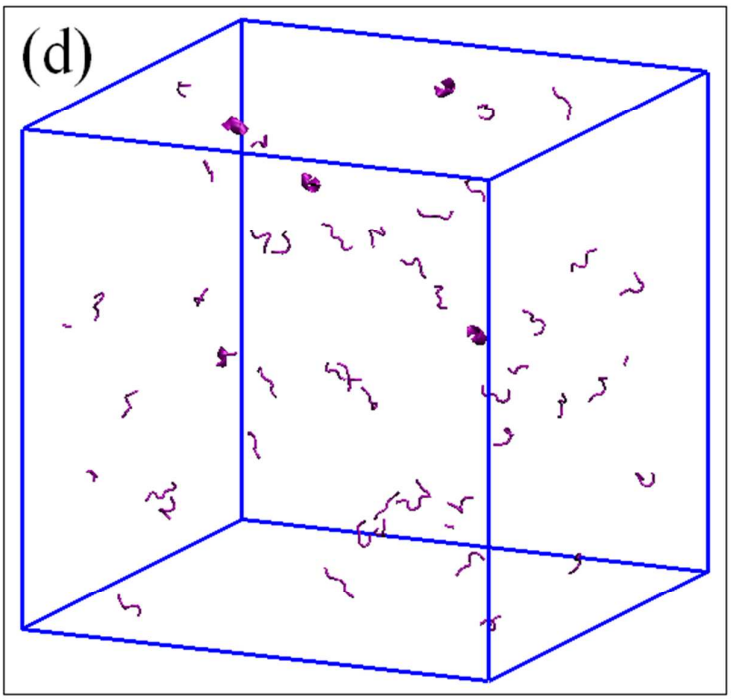

$T^* = 0.12$

Figure 3

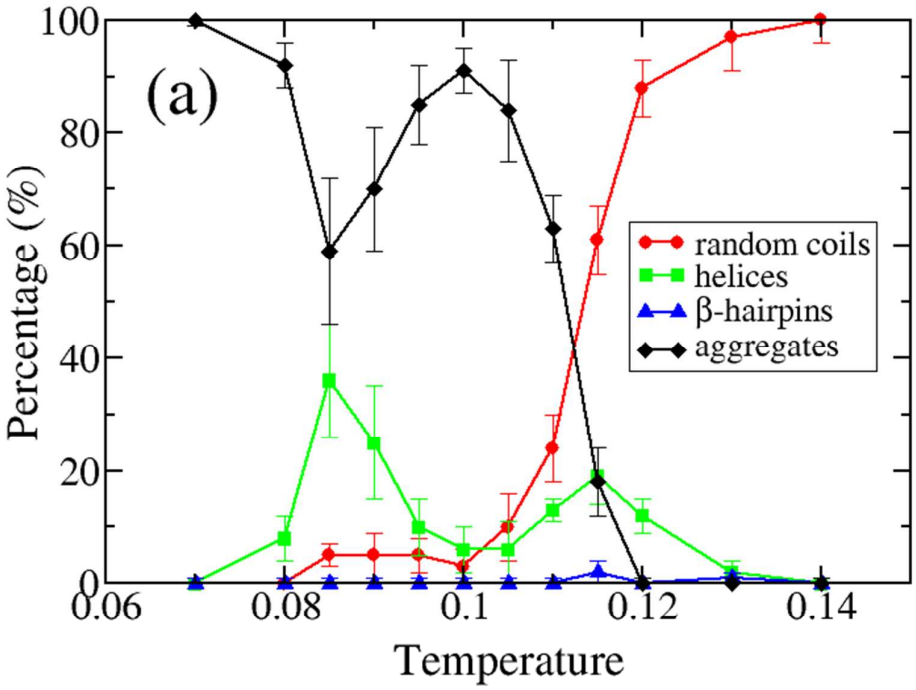

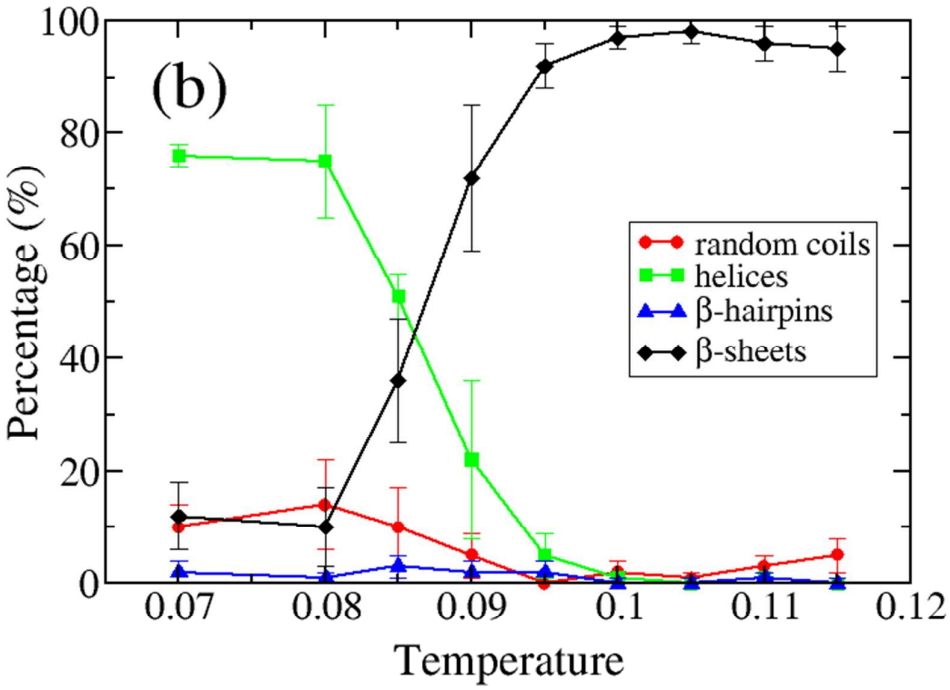

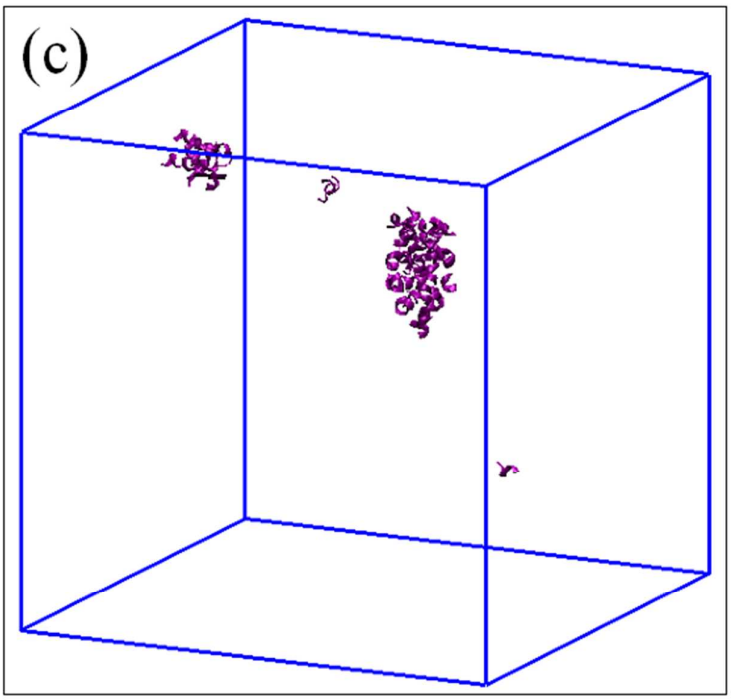

$T^* = 0.07$

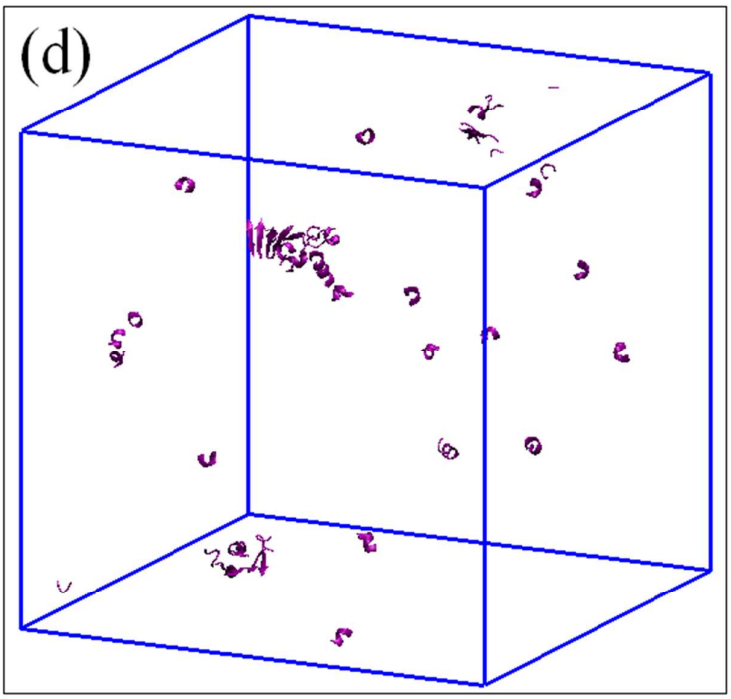

$T^* = 0.085$

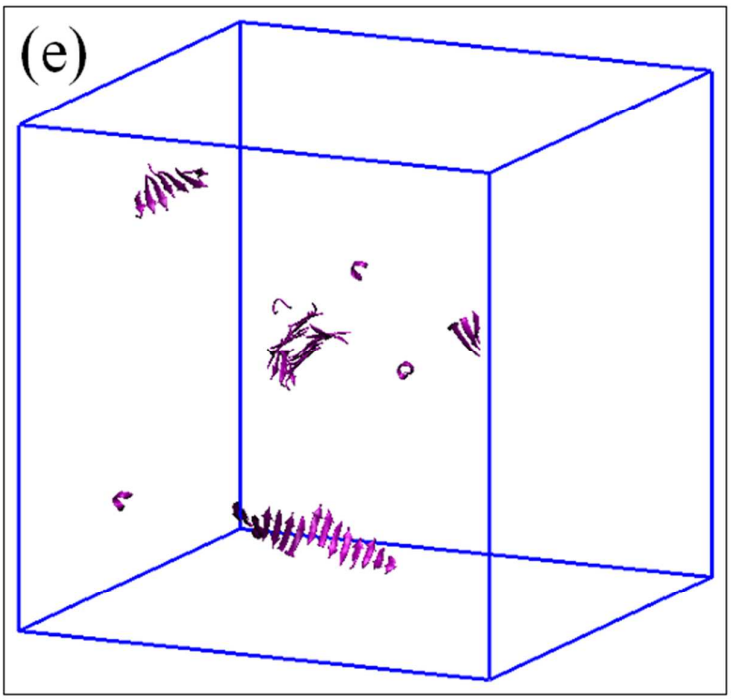

$T^* = 0.10$

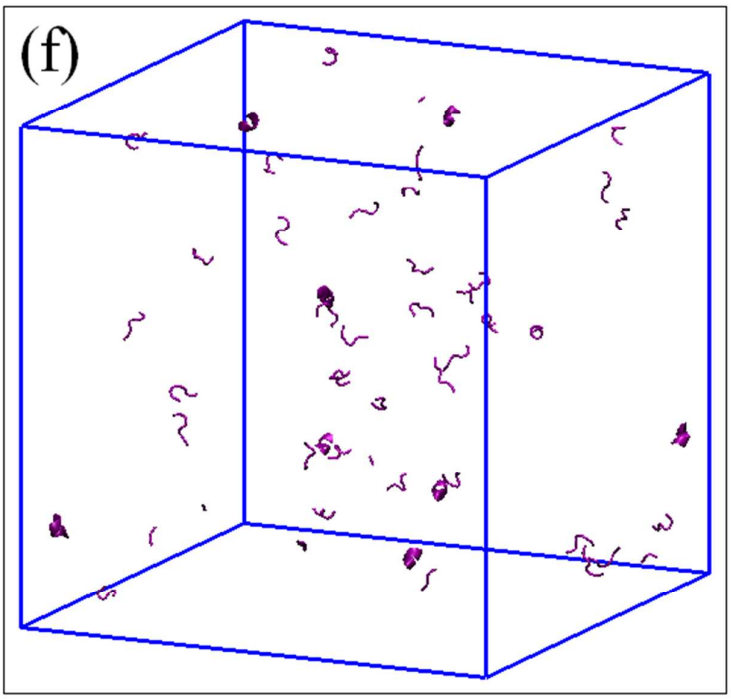

$T^* = 0.12$

Figure 4

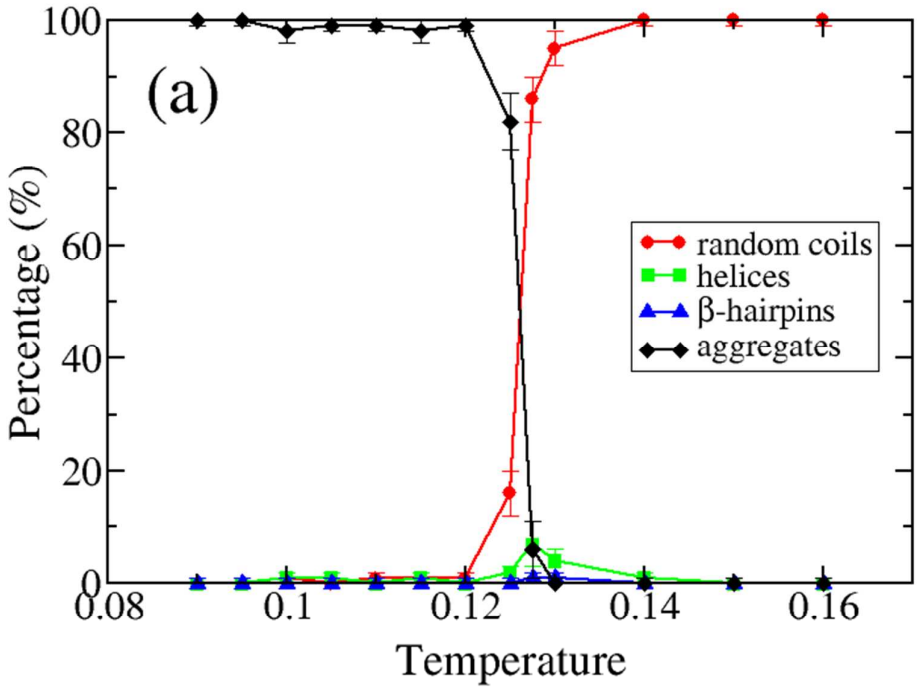

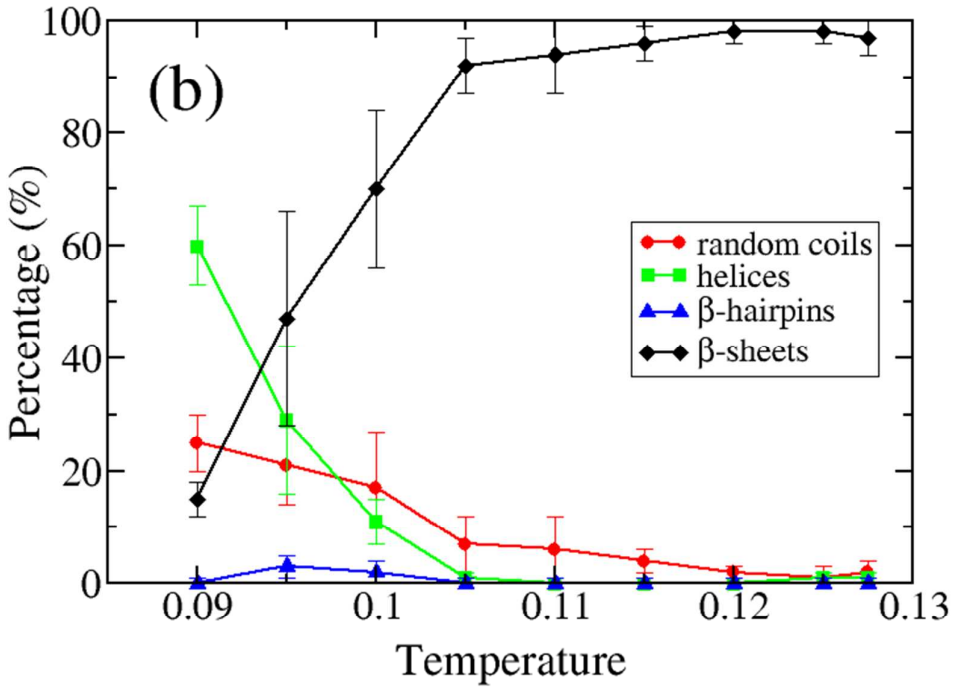

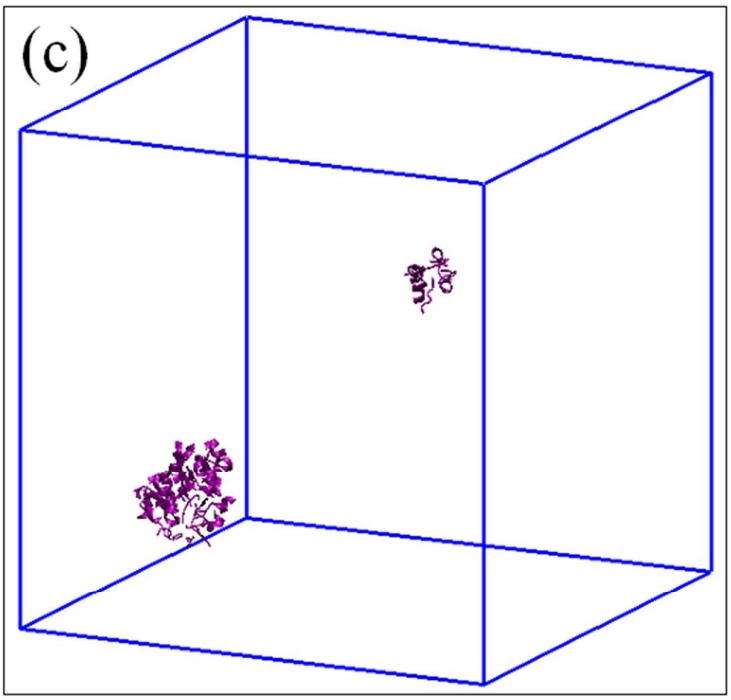

$T^* = 0.09$

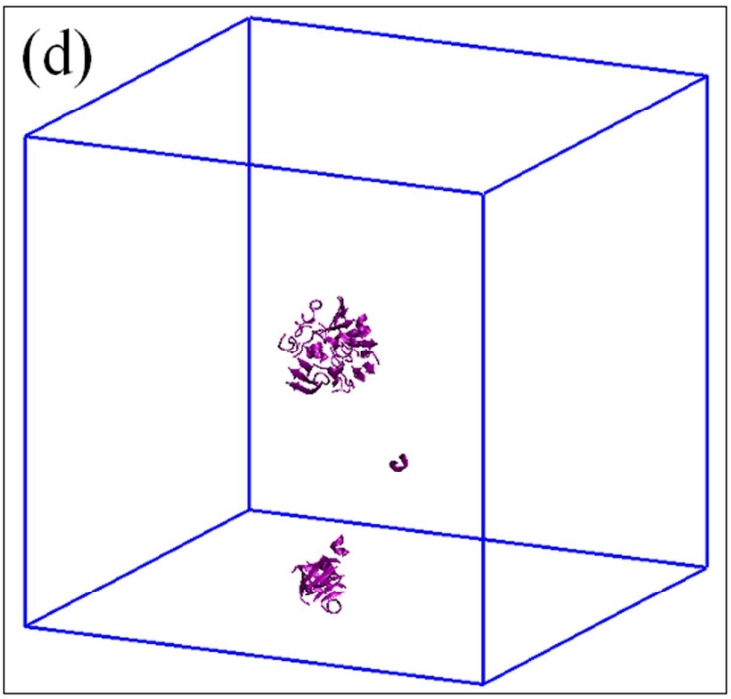

$T^* = 0.10$

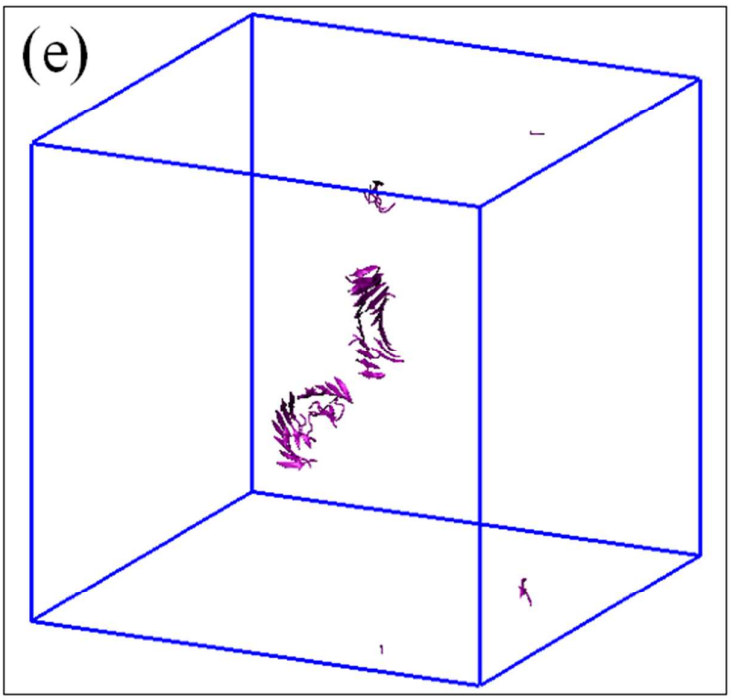

$T^* = 0.11$

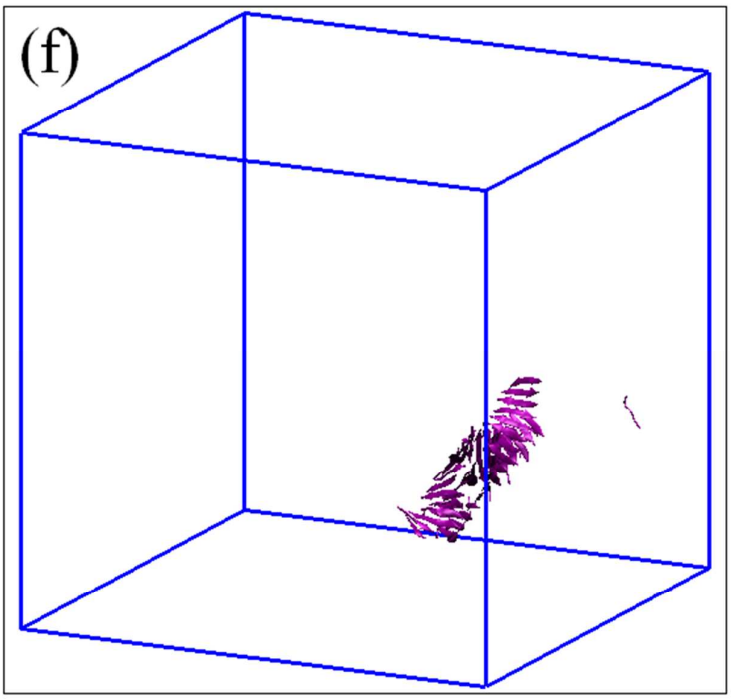

$T^* = 0.12$

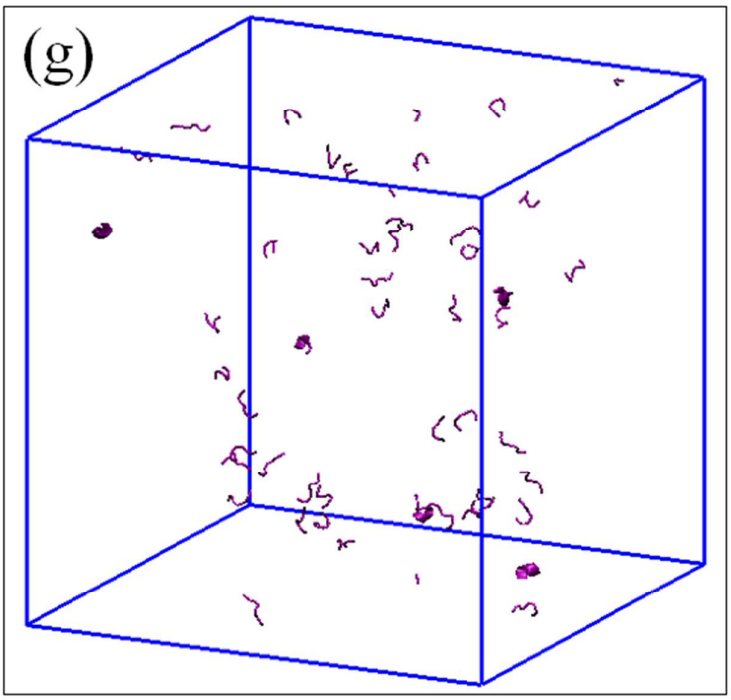

$T^* = 0.13$

Figure 5

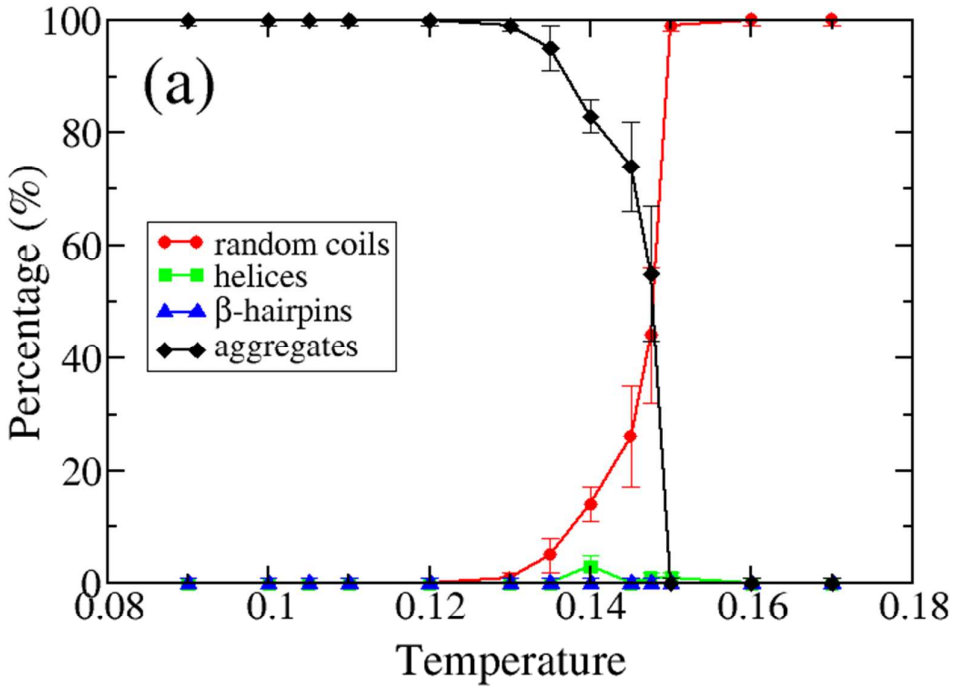

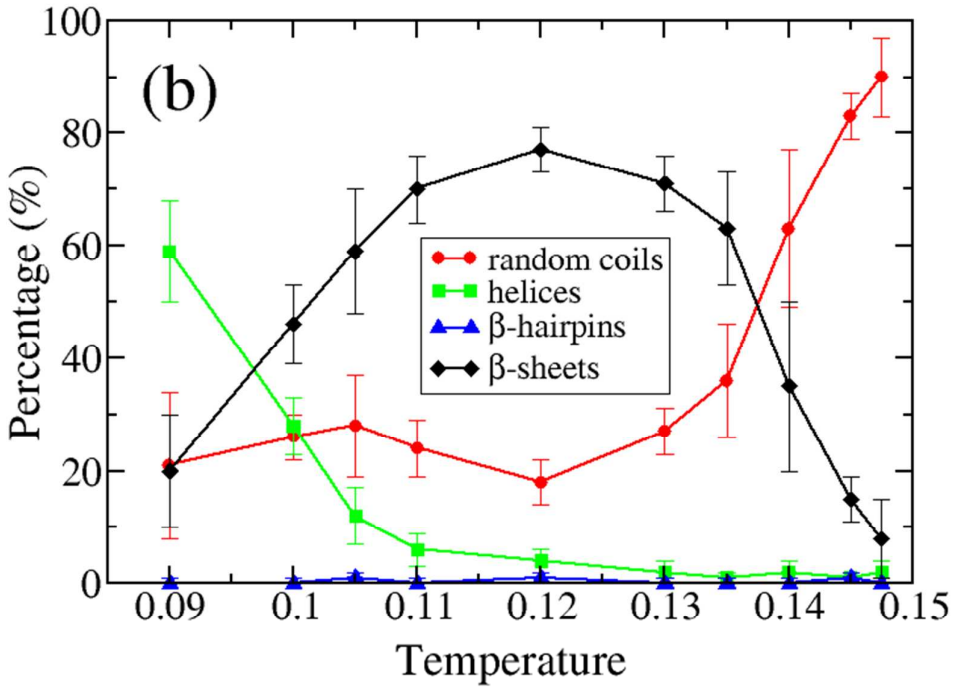

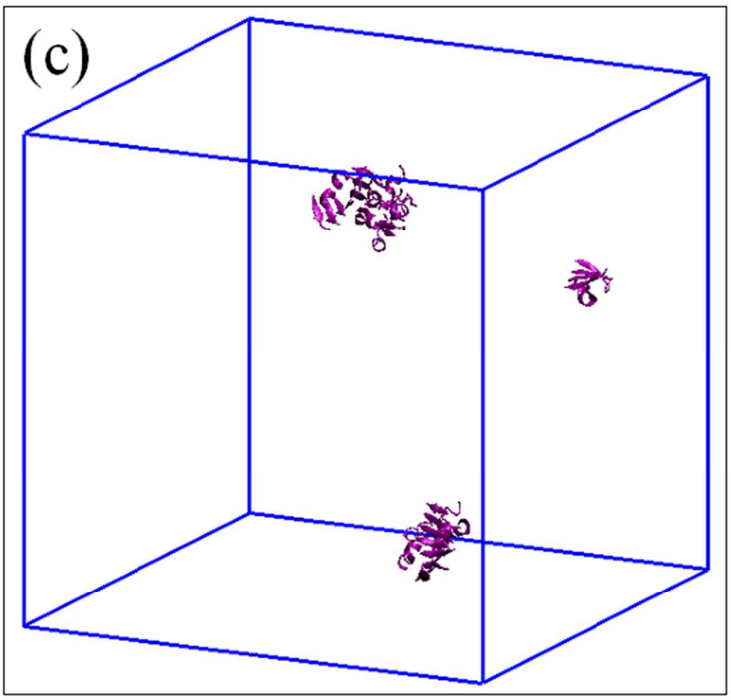

$T^* = 0.10$

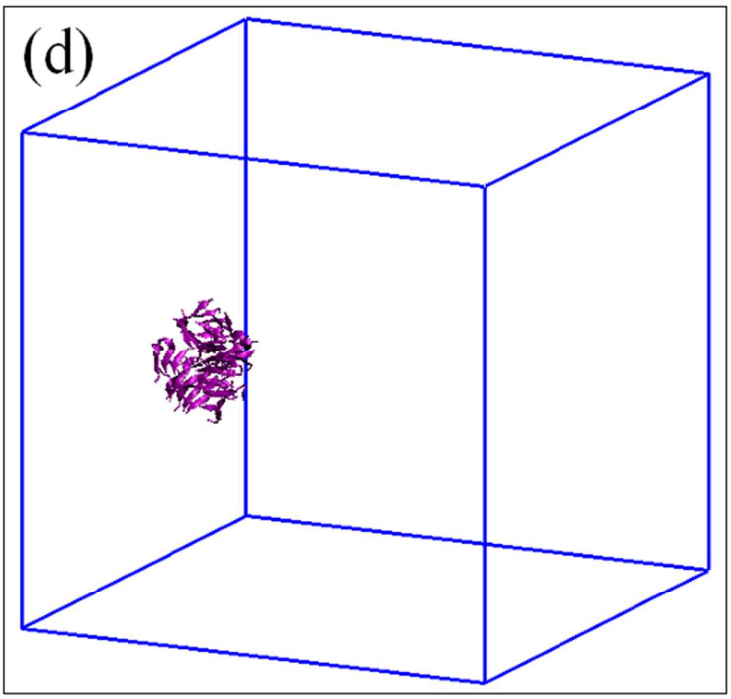

$T^* = 0.12$

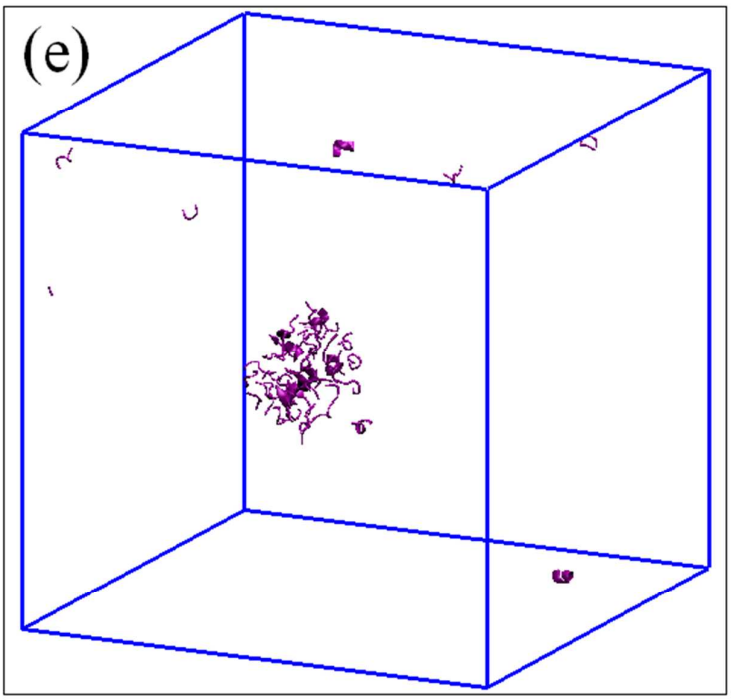

$T^* = 0.14$

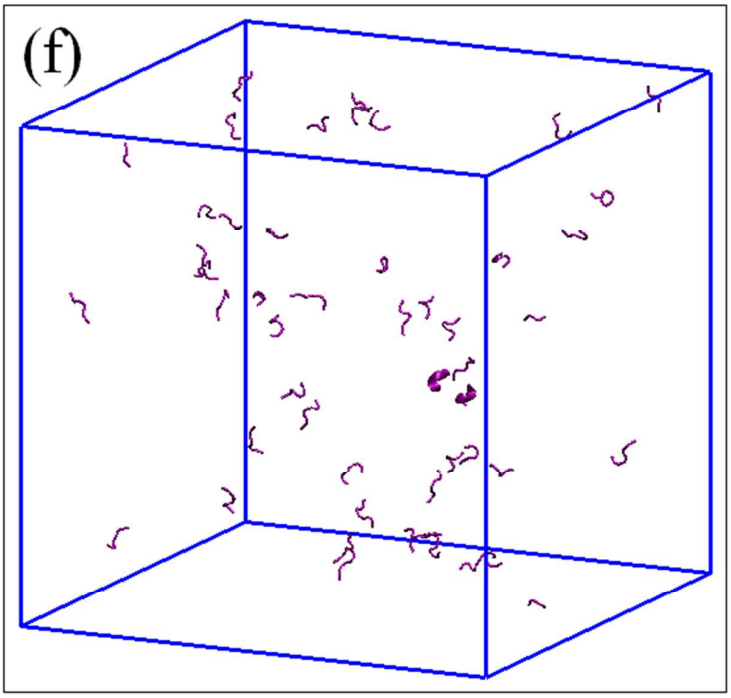

$T^* = 0.15$

Figure 6

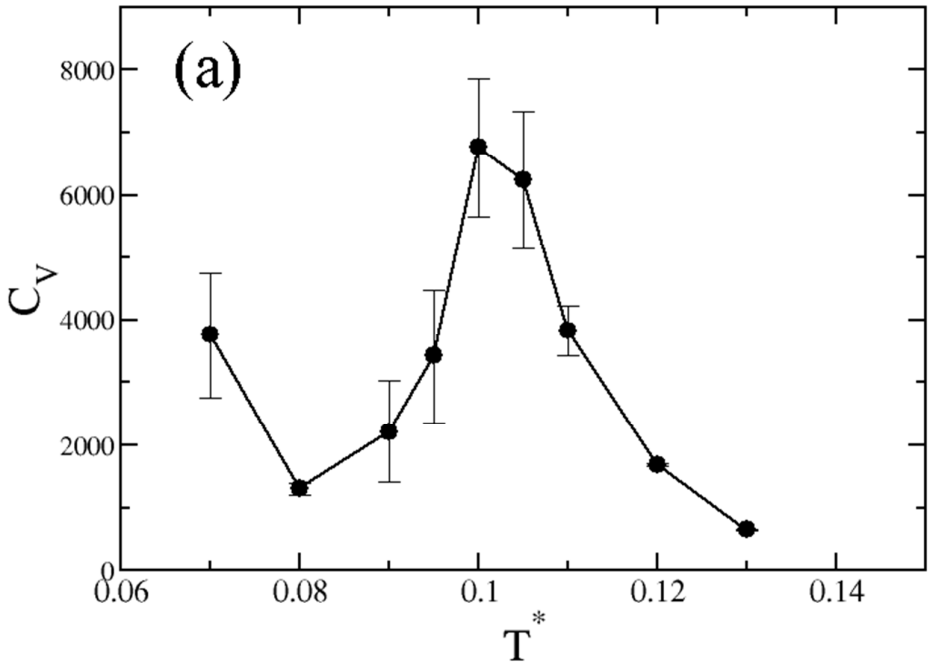

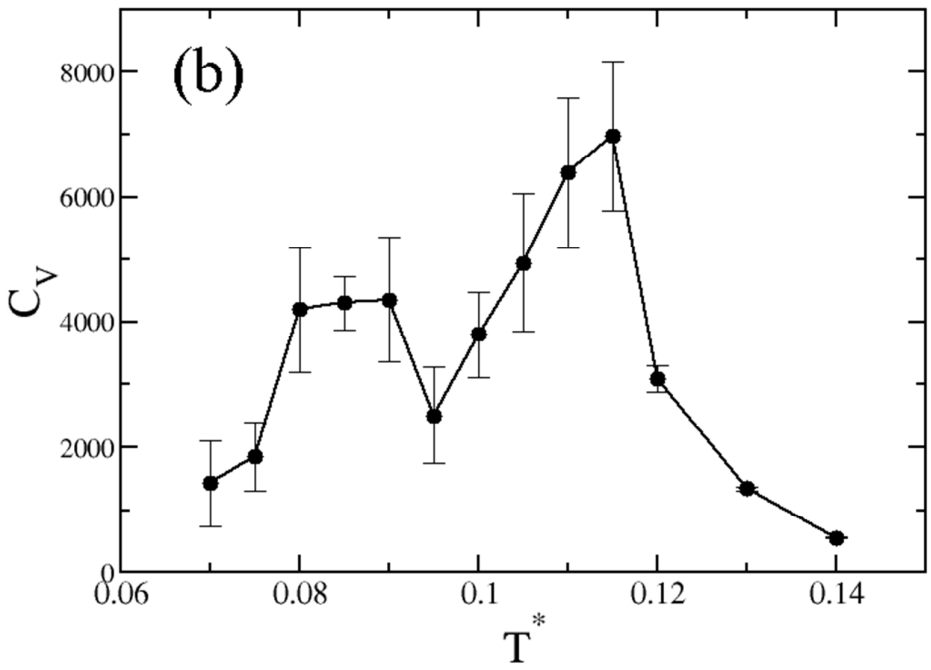

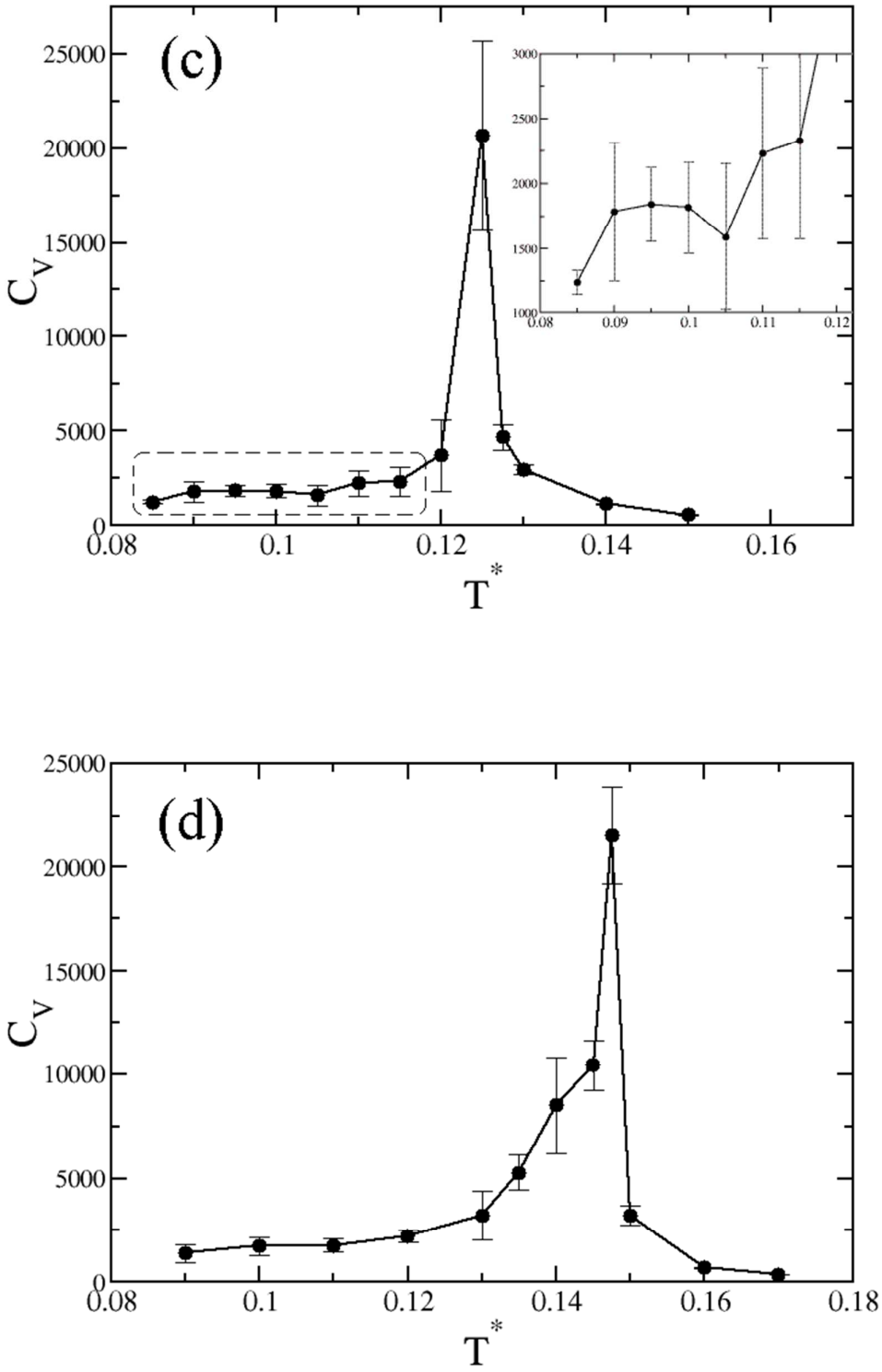

Figure 7

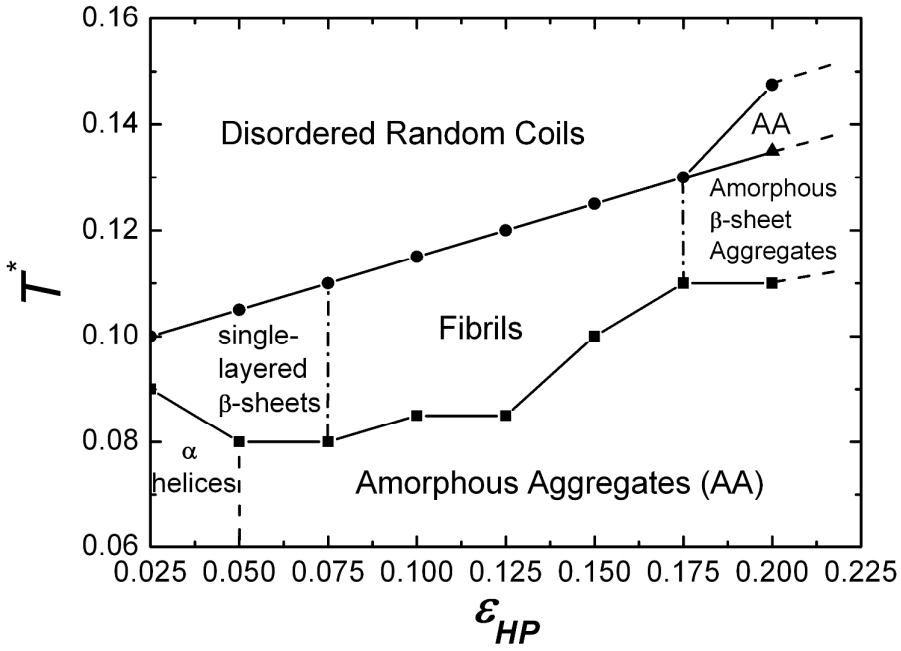

Figure 8

Rerferences:

1. C. M. Dobson, *Trends Biochem.Sci.*, 1999, **24**, 329-332.
2. J. W. Kelly, *Nature Structural Biology*, 2002, **9**, 323-325.
3. E. Zerovnik, *Eur. J. Biochem.*, 2002, **269**, 3362-3371.
4. F. Chiti and C. M. Dobson, in *Annual Review of Biochemistry*, Annual Reviews, Palo Alto, 2006, vol. 75, pp. 333-366.
5. P. T. Lansbury and H. A. Lashuel, *Nature*, 2006, **443**, 774-779.
6. M. Reches and E. Gazit, *Curr. Nanosci.*, 2006, **2**, 105-111.
7. J. D. Hartgerink, E. Beniash and S. I. Stupp, *Science*, 2001, **294**, 1684-1688.
8. A. Aggeli, M. Bell, N. Boden, J. N. Keen, P. F. Knowles, T. C. B. McLeish, M. Pitkeathly and S. E. Radford, *Nature*, 1997, **386**, 259-262.
9. J. D. Hartgerink, J. R. Granja, R. A. Milligan and M. R. Ghadiri, *J. Am. Chem. Soc.*, 1996, **118**, 43-50.
10. S. Vauthey, S. Santoso, H. Y. Gong, N. Watson and S. G. Zhang, *Proc. Natl. Acad. Sci. U. S. A.*, 2002, **99**, 5355-5360.
11. C. C. Cenker, S. Bucak and U. Olsson, *Soft Matter*, 2011, **7**, 4868-4875.
12. A. Mahler, M. Reches, M. Rechter, S. Cohen and E. Gazit, *Adv. Mater.*, 2006, **18**, 1365-+.
13. C. Sinthuvanich, L. A. Haines-Butterick, K. J. Nagy and J. P. Schneider, *Biomaterials*, 2012, **33**, 7478-7488.
14. T. C. Holmes, S. de Lacalle, X. Su, G. S. Liu, A. Rich and S. G. Zhang, *Proc. Natl. Acad. Sci. U. S. A.*, 2000, **97**, 6728-6733.
15. G. A. Silva, C. Czeisler, K. L. Niece, E. Beniash, D. A. Harrington, J. A. Kessler and S. I. Stupp, *Science*, 2004, **303**, 1352-1355.
16. R. G. Ellis-Behnke, Y. X. Liang, S. W. You, D. K. C. Tay, S. G. Zhang, K. F. So and G. E. Schneider, *Proc. Natl. Acad. Sci. U. S. A.*, 2006, **103**, 5054-5059.
17. Y. Nagai, L. D. Unsworth, S. Koutsopoulos and S. G. Zhang, *J. Control. Release*, 2006, **115**, 18-25.
18. F. Zhao, M. L. Ma and B. Xu, *Chem. Soc. Rev.*, 2009, **38**, 883-891.
19. S. Koutsopoulos, L. D. Unsworth, Y. Nagaia and S. G. Zhang, *Proc. Natl. Acad. Sci. U. S. A.*, 2009, **106**, 4623-4628.
20. T. J. Measey, R. Schweitzer-Stenner, V. Sa and K. Kornev, *Macromolecules*, 2010, **43**, 7800-7806.
21. J. F. Smith, T. P. J. Knowles, C. M. Dobson, C. E. MacPhee and M. E. Welland, *Proc. Natl. Acad. Sci. U. S. A.*, 2006, **103**, 15806-15811.
22. R. Fairman and K. S. Akerfeldt, *Curr. Opin. Struct. Biol.*, 2005, **15**, 453-463.
23. I. Cherny and E. Gazit, *Angew. Chem.-Int. Edit.*, 2008, **47**, 4062-4069.
24. K. Morris and L. Serpell, *Chem. Soc. Rev.*, 2010, **39**, 3445-3453.
25. X. B. Zhao, F. Pan, H. Xu, M. Yaseen, H. H. Shan, C. A. E. Hauser, S. G. Zhang and J. R. Lu, *Chem. Soc. Rev.*, 2010, **39**, 3480-3498.
26. P. Sikorski, E. D. T. Atkins and L. C. Serpell, *Structure*, 2003, **11**, 915-926.
27. T. Luhrs, C. Ritter, M. Adrian, D. Riek-Loher, B. Bohrmann, H. Doeli, D. Schubert and R.

Riek, *Proc. Natl. Acad. Sci. U. S. A.*, 2005, **102**, 17342-17347.

28. P. Sikorski, M. Wada, L. Heux, H. Shintani and B. T. Stokke, *Macromolecules*, 2004, **37**, 4547-4553.
29. K. C. Holmes, D. Popp, W. Gebhard and W. Kabsch, *Nature*, 1990, **347**, 44-49.
30. T. Oda, M. Iwasa, T. Aihara, Y. Maeda and A. Narita, *Nature*, 2009, **457**, 441-445.
31. D. Papapostolou, A. M. Smith, E. D. T. Atkins, S. J. Oliver, M. G. Ryadnov, L. C. Serpell and D. N. Woolfson, *Proc. Natl. Acad. Sci. U. S. A.*, 2007, **104**, 10853-10858.
32. M. R. Dreher, A. J. Simnick, K. Fischer, R. J. Smith, A. Patel, M. Schmidt and A. Chilkoti, *J. Am. Chem. Soc.*, 2008, **130**, 687-694.
33. Y. Qiao, Y. Y. Lin, Z. Y. Yang, H. F. Chen, S. F. Zhang, Y. Yan and J. B. Huang, *J. Phys. Chem. B*, 2010, **114**, 11725-11730.
34. R. Sabate, A. Villar-Pique, A. Espargaro and S. Ventura, *Biomacromolecules*, 2012, **13**, 474-483.
35. J. Zurdo, J. I. Guijarro, J. L. Jimenez, H. R. Saibil and C. M. Dobson, *J. Mol. Biol.*, 2001, **311**, 325-340.
36. Y. S. Hong, R. L. Legge, S. Zhang and P. Chen, *Biomacromolecules*, 2003, **4**, 1433-1442.
37. Y. Zimenkov, S. N. Dublin, R. Ni, R. S. Tu, V. Breedveld, R. P. Apkarian and V. P. Conticello, *J. Am. Chem. Soc.*, 2006, **128**, 6770-6771.
38. K. Giri, N. P. Bhattacharyya and S. Basak, *Biophys. J.*, 2007, **92**, 293-302.
39. B. Ozbas, J. Kretsinger, K. Rajagopal, J. P. Schneider and D. J. Pochan, *Macromolecules*, 2004, **37**, 7331-7337.
40. Y. Hong, M. D. Pritzker, R. L. Legge and P. Chen, *Colloid Surf. B-Biointerfaces*, 2005, **46**, 152-161.
41. V. Castelletto, I. W. Hamley, C. Cenker and U. Olsson, *J. Phys. Chem. B*, 2010, **114**, 8002-8008.
42. W. Hwang, B. H. Kim, R. Dandu, J. Cappello, H. Ghandehari and J. Seog, *Langmuir*, 2009, **25**, 12682-12686.
43. G. Demirel and F. Buyukserin, *Langmuir*, 2011, **27**, 12533-12538.
44. P. Kumaraswamy, R. Lakshmanan, S. Sethuraman and U. M. Krishnan, *Soft Matter*, 2011, **7**, 2744-2754.
45. L. Zhang, J. Zhong, L. X. Huang, L. J. Wang, Y. K. Hong and Y. L. Sha, *J. Phys. Chem. B*, 2008, **112**, 8950-8954.
46. J. T. Meijer, M. Roeters, V. Viola, D. W. P. M. Lowik, G. Vriend and J. C. M. van Hest, *Langmuir*, 2007, **23**, 2058-2063.
47. S. Han, S. Cao, Y. Wang, J. Wang, D. Xia, H. Xu, X. Zhao and J. R. Lu, *Chemistry-a European Journal*, 2011, **17**, 13095-13102.
48. W. M. Berhanu and U. H. E. Hansmann, *Protein Science*, 2012, **21**, 1837-1848.
49. L. N. Zhao, Y. Mu and L. Y. Chew, *Physical Chemistry Chemical Physics*, 2013, **15**, 14098-14106.
50. R. Ni, S. Abeln, M. Schor, M. A. C. Stuart and P. G. Bolhuis, *Phys Rev Lett*, 2013, **111**.
51. S. Takada, Z. Luthey-Schulten and P. G. Wolynes, *Journal of Chemical Physics*, 1999, **110**, 11616-11629.
52. A. V. Smith and C. K. Hall, *Proteins*, 2001, **44**, 344-360.
53. N. Y. Chen, Z. Y. Su and C. Y. Mou, *Phys Rev Lett*, 2006, **96**.

54. Y. Mu and Y. Q. Gao, *Physical Review E*, 2009, **80**.
55. Y. Mu, *Physical Review E*, 2011, **84**.
56. M. R. Betancourt, *Journal of Chemical Physics*, 2005, **123**.
57. L. D. Landau and E. M. Lifshitz, *Statistical Physics* (Butterworth-Heinemann, Oxford, 1980).
58. H. D. Nguyen and C. K. Hall, *J. Am. Chem. Soc.*, 2006, **128**, 1890-1901.
59. J. P. Bernacki and R. M. Murphy, *Biochemistry*, 2011, **50**, 9200-9211.
60. S. E. Blondelle, B. Forood, R. A. Houghten and E. PerezPaya, *Biochemistry*, 1997, **36**, 8393-8400.
61. T. D. Do, N. J. Economou, N. E. LaPointe, W. M. Kincannon, C. Bleiholder, S. C. Feinstein, D. B. Teplow, S. K. Buratto and M. T. Bowers, *J. Phys. Chem. B*, 2013, **117**, 8436-8446.